X RAY AND INFRARED SELECTED AGN.-II. OPTICAL SPECTROSCOPY

S. D. KIRHAKOS
Departamento de Astrofísica, Instituto de Pesquisas Espaciais, C. P. 515, 12201 São José dos Campos, São Paulo, Brazil
and
Cerro Tololo Inter-American Observatory, National Optical Astronomy Observatories,[a] Casilla 603, La Serena, Chile

J. E. STEINER[b), c)]
Departamento de Astrofísica, Instituto de Pesquisas Espaciais, C. P. 515, 12201 São José dos Campos, São Paulo, Brazil
Received 29 September 1989; revised 13 February 1990

ABSTRACT

In a search for obscured active galactic nuclei we selected 144 x-ray/infrared emitting galaxies. Optical spectroscopy of this sample is presented. A classification according to the nuclear activity shows that 28 are AGN, 39 are transition-type objects and 44 are H II region-like galaxies. Three of the 28 AGN are Seyfert 1 galaxies and the others are of Type 2. We suggest that the objects identified as narrow line AGN are obscured Seyfert 1. Most of the observed galaxies are seen edge-on, indicating that dust may have a flattened distribution coplanar to the disk of the parent galaxy. With the inclusion of the newly identified AGN, the sample of the x-ray emitting Seyfert 2 galaxies is fairly complete above a flux limit of $\log F_{Hx} \sim -10.8$.

I. INTRODUCTION

Active galactic nuclei (AGN) are known to emit continuum spectra in form of a power law. For this reason, most of the nearby AGN can be detected from x rays to infrared, including the ultraviolet and optical spectral regions. This property has been used in surveys to find more of these objects. The x-ray satellites UHURU and Ariel V, for example, showed that x-ray emission is a powerful signal of nuclear activity and is very useful for identifying new AGN (Elvis *et al.* 1978; Wilson 1979). This technique led to the discovery of narrow emission-line x-ray emitting galaxies (Ward *et al.* 1978; Schnopper *et al.* 1978; Bradt *et al.* 1978). More detailed optical studies showed that they are, in fact, obscured type 1 Seyfert galaxies (Sy 1) (Shuder 1980; Véron *et al.* 1980; Lawrence and Elvis 1982).

In the infrared region there is only one recent satellite (*IRAS*) with sufficient sensitivity to detect large numbers of AGN. The *IRAS* measurements showed that AGN are strong sources of infrared emission (Miley *et al.* 1985). On the basis of *IRAS* data, some successful programs have been carried out to find new AGN (Carter 1984; Osterbrock and de Robertis 1985; de Grijp *et al.* 1985, 1987; Kailey and Lebofsky 1988; Low *et al.* 1988).

The present work was motivated by the fact that many of the edge-on Seyfert galaxies are missing from optical surveys (Keel 1980). The scarcity of edge-on objects is noted among Sy 1 as well as among Sy 2 (Kirhakos 1986 and Paper I). A plausible explanation is absorption by dust in the plane of spiral galaxies and/or in a region near the nucleus, aligned with the galactic plane (Lawrence and Elvis 1982).

One way to select obscured active nuclei is to look for infrared and hard x-ray emission, since photons from these spectral bands are not absorbed by dust. For the present investigation we selected infrared emitting galaxies detected by *IRAS* (Lonsdale *et al.* 1985) that lie close to or inside the error boxes of unidentified hard x-ray sources (Wood *et al.* 1984). 144 galaxies were selected by this criterion (see Paper I for more details). In the present paper we show and discuss spectroscopic measurements for this sample of galaxies.

II. OBSERVATIONS

Spectrophotometric observations of the nuclei of the selected galaxies were taken at the 1 m telescope of the CTIO (Cerro Tololo Interamerican Observatory) with the Cassegrain spectrograph and two-dimensional photon counting detector (2D-Frutti). In those cases in which more than one galaxy was close to the coordinates of the *IRAS* source, spectra were taken for all of them. On the other hand, we were not able to get spectra of seven very faint galaxies and two others were not observed due to weather conditions. The total number of objects observed is 146.

The data were collected in November 1986 and between May 1987 and April 1988. The observed wavelength range was 3900 to 7000 Å with a spectral resolution of ~ 5 Å. A 600 1/mm grating was used with an effective blaze at 5000 Å. The galaxies were observed through a slit 200–250 μm (4–5 arcsec) wide. The exposure times range from 1800 to 7200 s.

About four standard stars (Stone and Baldwin 1983; Baldwin and Stone 1984) were observed each night to provide flux calibration. The slit was opened to 12 arcsec (600 μm) to observe the standard stars. Most of the nights were photometric and the seeing was between 1 and 3 arcsec.

The 2D-Frutti spectra are highly distorted due to the image tubes. To correct for this, we took multihole and long arc exposures (1000 s) each night before starting the observations. The distortions were mapped through the multihole and arc frames and the resulting bidimensional solution was used to rectify the images. The distortion-corrected images have constant scale through the slit direction and are linear in wavelength. Dome flats of a quartz lamp were taken each afternoon to map out the relative response of the detector in each pixel, and sky-flat frames were obtained during the twi-

[a] Cerro Tololo Inter-American Observatory, National Optical Astronomy Observatories, is operated by the Association of Universities for Research in Astronomy, Inc., under contract with the National Science Foundation.
[b] On leave from IAG–Universidade de São Paulo, C. P. 30627, Sao Paulo, Brazil.
[c] Visiting Astronomer, Cerro Tololo Inter-American Observatory.

 0004-6256/90/061722-18$00.90

light to verify the uniformity of the slit illumination. Long dark exposures (10 000 s) were taken in the mornings. After observing each galaxy, a short arc exposure of a He–Ar lamp was taken in order to obtain accurate radial velocities.

The flatfield operation was done by subtracting the scaled dark frame from the flat and dividing all images by the resulting flat frame. Once the spectra were corrected for distortion and flatfield, the one-dimensional spectra were extracted. After that, wavelength calibration and atmospheric extinction correction were applied. Finally, using the standard stars, calibration curves were obtained for each night (or group of nights) and the observed spectra of the galaxies were flux calibrated. All steps in the data reduction procedure, from distortion correction up to flux calibration, and the analysis of the spectra were done using IRAF routines and computer facilities at CTIO.

CCD frames in the *UBVRI* system were taken for most of the galaxies with the 91 cm telescope at CTIO. An analysis of these observations will be published elsewhere.

III. ANALYSIS AND RESULTS

a) Line Measurements

The redshifts of the emission-line galaxies were computed as a weighted mean considering the redshifts of all measurable emission lines in the spectra and their equivalent width as the relative weight. No heliocentric correction was applied. Redshifts from absorption lines were obtained in the cases where these were the only lines present in the spectrum. Redshifts are listed in Tables I(a), II(a), III(a), and IV. A Gaussian fit to the emission lines was used to determine their width and flux, and the local continuum was set by visual inspection of the spectra. The observed full width at half maximum (FWHM) is the actual width convolved with the

TABLE I(a). Galaxies classified as AGNs.

IRAS galaxy	HEAO-1 source	z	FWHM [OIII]	FWHM H_α	[NII]/H_α	H_α/H_β	[OIII]/H_β	[SII]/H_α
01065-4644	1H0102-469	.0325(1)	384	513	0.18	7.3	0.9	0.2
01173+1431	1H0112+141	.0137(2)	361	311	0.67	9.2	0.8	0.4:
01363-4016	1H0137-403	.0252(3)	408	169	<1.08:			
02578-1100A	1H0301-106	.0324(1)	423	2234	0.22:	>8.0[b]	17.0:	
03012-0117	1H0258-015	.0134(2)	396	230	<1.02:			
04235-0840B	1H0422-086	.0392(3)	<484	305	0.57	11.5	0.9	
04461-0624	1H0445-060	.0152(1)	443	233	0.98	15.1	7.1	0.4
04575-7537	1H0502-755	.0186(1)	507	465	1.88	3.9	7.1	0.7:
08594-2435	1H0857-242	.0259(3)	<134	>314	0.70			
08599+1102	1H0856+108	.0151(4)	304	252	0.28	5.3	0.6	0.1[a]
09166-3747	1H0910-374	.0083(3)			>1.5 :			>1.0:
09250+1230B	1H0929+122	.0290(5)		329	0.68			
09530+0517	1H0951+057	.0348(4)		352	0.31	10.1		0.3[a]
10329-1352	1H1032-142	.0155(7)	400	302	1.60			
11184-4259	1H1118-431	.0566(1)	425	1744	?	4.2[b]	1.0	
11186-0242	1H1117-026	.0247(1)		>428	0.65			
13025-4911[c]	1H1304-497							
13028-4909[c]	1H1304-497	.0012(8)		161	1.28:			
13042-2338	1H1308-237	.0097(1)	455	333	1.19	7.1	10.0	0.4
13044-2324	1H1308-237	.0097(1)	383	>351	1.11	7.0	1.6	0.4
14095-2652	1H1409-267	.0223(3)	243	234	1.45			
14110+0912	1H1411+094	.0239(3)	349	219	0.38	8.2	2.1	
15115-4009A	1H1513-400	.0237(3)	262	3081	?	5.0[b]	0.3	
15374-1817	1H1538-182	.0235(3)	384	505	0.54	9.0	1.2	
19393-5846	1H1930-589	.0069(3)	304	263	0.62	12.7	0.6	0.3
20559-5251	1H2100-526	.0240(3)	339	299	0.64	10.0	1.7	
21116+0158	1H2108+019	.0131(4)	313?	474	1.38			
22547-8018	1H2253-810	.037 (1)		375	0.41	13.1		
23031-3052	1H2308-309	.0286(2)	472	280	0.48	8.1		0.3

Notes:
a) only [SII] λ6717Å measured
b) broad components
c) two IRAS sources in the same galaxy

TABLE I(b). Galaxies classified as AGNs.

IRAS galaxy	b/a	Flux Densities (Janskys) 12μm	25μm	60μm	100μm	Log L_{HX}	Log $L_{H\alpha}$	Log L_{IR}
01065-46	0.94	0.25L	0.25L	0.99	2.24	44.03	42.15	44.45
01173+14	0.85	0.28L	0.44:	2.80	3.75	42.97	40.80	44.05
01363-40	0.23	0.39L	0.24L	0.60	2.14	43.44	40.54	44.11
02578-11A	0.50	0.25L	0.26L	0.72	1.32	43.73	41.77	44.27
03012-01	0.53	0.31:	0.54	0.78	1.00L	43.08	39.79	43.46
04235-08B	0.74	0.26L	0.25L	0.89	3.13	44.10	41.47	44.46
04461-06	0.80	0.40	0.67	5.77	14.21	43.28	40.86	44.57
04575-75	0.75	0.57	0.45	0.70	1.48	43.69	40.62	43.79
08594-24	0.57	0.25L	0.25L	1.08	2.67	43.78	40.81	44.30
08599+11	0.39	0.25L	0.28L	0.67	1.15	43.36	40.68	43.60
09166-37	0.44	0.25L	0.25L	0.60L	3.64	42.75		42.66
09250+12B	0.29:	0.25L	0.33L	1.40	3.03	43.82	40.62	44.49
09530+05	0.40	0.48L	0.60L	0.45	1.05	43.99	41.11	44.17
10329-13	0.25	0.25L	0.25L	0.50:	1.45	43.29	40.11	43.55
11184-42	0.56	0.25L	0.34	0.57	1.00L	44.30	42.38	45.38
11186-02	0.74	0.33	0.75	5.38	8.85	43.71	41.42	44.88
13025-49[a]	0.17	3.65	14.32	388.05	684.01			44.14
13028-49[a]	0.17	0.69	0.89	4.75:	1.05L	40.96	38.26	42.04
13042-23	0.54	0.25L	0.25L	0.83	2.03	42.95	40.47	43.34
13044-23	0.47	0.40:	1.26	2.30	3.23	42.95	40.60	43.68
14095-26	0.91	0.25L	0.26L	1.49	3.59	43.64	40.36	43.36
14110+09	0.39	0.96L	0.25L	0.55	1.01L	43.88	40.73	43.88L
15115-40A	0.30	1.05	0.43:	0.40L	1.99L	43.83	41.92	44.92
15374-18	0.94	0.29L	0.33L	0.56	1.90	43.63	40.64	44.00
19393-58	0.27	1.06	3.51	17.84	33.65	42.63	40.45	44.32
20559-52	0.22	0.25L	0.35	2.00	3.15	43.76	40.93	44.42
21116+01	0.33	0.25L	0.60	3.81	6.56	43.45	39.98	44.18
22547-80	0.26	0.25L	0.25L	1.21	3.21	43.86	40.96	44.68
23031-30	0.19pec	0.32L	0.41:	3.02	4.33	43.46	41.27	44.73

Notes:
a) two IRAS sources in the same galaxy

TABLE II(a). Galaxies classified as transition type objects.

IRAS galaxy	HEAO-1 source	z	FWHM [OIII]	H_α	[NII]/H_α	H_α/H_β	[OIII]/H_β	[SII]/H_α
00141+0647	1H0017+073	.0132(3)		172	0.73			
01043+0140	1H0102+017	.0156(1)	292	>198	0.36	6.6		0.2
01161+1443	1H0112+141	.0231(3)		84	0.71			
01356-4047	1H0137-403	.0050(1)	235	134	0.16	6.2	2.0	0.4
01358-4019	1H0137-403	.0199(2)		206	0.33	10.1		0.2[a]
02078-1033	1H0208-106	.0133(2)	<130	217	0.53	9.3	1.2	
02543+0600	1H0253+058	.0211(2)		206	0.48			
02558+0606	1H0253+058	.0235(3)		271	0.39	18.7		
02578-1100B	1H0301-106	.0335(3)	259	285	0.37	5.7	0.5	
03004-0134	1H0258-015	.0288(2)	256	142	0.45	9.0	1.7	
03018-5041	1H0307-499	.021 (1)		317:	1.0?			
03141-3432	1H0311-348	.0164(3)		<90	0.76			
04381-2713	1H0435-274	.0838(2)		300:	0.29	11.1		
04455-5641	1H0451-560	.0411(4)	<127	202	0.61	7.9	0.7	
04493-0553	1H0445-060	.0091(1)	238	118	0.37	4.3	0.6	0.4
05121-4905	1H0515-488	.0484(1)	287	149	0.31	3.5	2.0	
05174+0631	1H0516+063	.0298(4)		272	0.92	5.0		
05431-4347	1H0546-439	.0458(4)		>200	0.52	5.0		
05455-8200	1H0551-819	.016 (3)		326:				
07395-6755A	1H0737-668	.0373(5)	286	<101	0.64	5.0	1.8	
07395-6755B	1H0737-668	.0369(5)[b]	333:				0.4	
07398+1826	1H0743+184	.028 (2)		202	0.64			
08455-7845	1H0834-793	.018 (1)		257				
09060-3721	1H0910-374	.0188(3)	403:	349:	0.22:	15.0	2.1	
09250+1230A	1H0929+122	.0288(5)		161	0.72			
09263-3554B	1H0926-362	.0161(8)		231	0.83			
09321+1030	1H0932+107	.0082(6)		212	0.51			
11013-2258	1H1100-230	.0038(1)	<368	165	0.36	4.9	0.5	0.5
11203-0238	1H1117-026	.0456(3)		>241	0.57			
11203-4343	1H1118-431	.0175(3)		226	0.40	8.3		0.3[a]
11206-4304	1H1118-431	.0174(2)		243	0.43	9.3		0.4[a]
13071-2358	1H1308-237	.0110(9)	207	165	0.16	6.6	3.4	
13220+0647	1H1320+066	.022 (2)		280				
13228-2423	1H1325-246	.033 (2)		290	0.55			
13301-2455	1H1325-246	.0261(4)		112	0.72	5.0		
14255+0113	1H1427+013	.0255(1)	419:	199	0.38	7.0	0.8	0.3
16065-2825A	1H1611-286	.0144(7)		289	0.29	11.7		0.2[a]
16065-2852B	1H1611-286	.0142(4)		136	0.60	6.6		
20459-2214	1H2048-224	.026 (8)		245				

Notes:
a) only [SII] λ6717Å measured.
b) spectra taken do not cover H_α region.

TABLE II(b). Galaxies classified as transition type objects.

IRAS galaxy	b/a	Flux Densities (Janskys) 12μm	25μm	60μm	100μm	Log L_{HX}	Log $L_{H\alpha}$	Log L_{IR}
00141+06	0.21	0.29L	0.29L	2.32	5.09	43.09	40.22	44.02
01043+01	0.8 :	0.77L	0.34L	1.98	2.53	43.20	40.72	44.01
01161+14	0.74	0.25L	0.26L	0.74	1.68	43.42	40.86	44.02
01356-40	0.22	0.47L	0.36L	0.50	1.84L	42.03	39.69	42.63
01358-40	0.20	0.25L	0.35L	0.85	2.10	43.23	40.61	43.97
02078-10	0.48	0.27L	0.45L	1.40	3.04	43.01	40.46	43.81
02543+06	0.53	0.25L	0.29L	1.24	2.19	43.89	40.43	44.12
02558+06	0.43	0.25L	0.29L	1.38	3.23	43.99	40.37	44.37
02578-11B	0.72						41.33	
03004-01	0.43	0.25L	0.28L	0.61	1.33	43.75	40.93	44.12
03018-50	0.11	0.25L	0.24L	0.92	2.32	43.64	39.96	44.06
03141-34	0.42	0.39L	0.25L	0.63	1.89	43.39	40.10	43.71
04381-27	0.70	0.27L	0.25L	0.55	1.17	44.87	41.87	45.00
04455-56	0.53	0.25L	0.25L	0.60	1.27	43.88	41.13	44.42
04493-05	0.96	0.25L	0.30	2.44	4.72	42.84	40.62	43.71
05121-49	0.25	0.56L	0.30L	0.91	1.48	44.24	41.83	44.69
05174+06	0.29	0.42L	0.25L	0.79	5.45L	43.90	40.99	44.56
05431-43	0.41	0.25L	0.25L	0.56	1.01L	44.12	41.04	44.48
05455-82	0.55	0.90L	0.50L	0.48	1.70L	43.22	39.86	43.61
07395-67A	0.31:	0.25L	0.25L	0.81	1.29:	43.93	40.80	44.40
07395-67B	0.13	0.25L	0.25L	0.81	1.29:	43.92		44.40
07398+18	0.20	0.27L	0.32L	0.51	1.40:	43.91	40.36	44.08
08455-78	0.39	0.25L	0.25L	0.44	2.20	42.89	40.29	43.72
09060-37	0.69	0.42L	0.25L	0.68	7.06L	43.46	40.57	44.23
09250+12A	0.29:						40.73	
09263-35B	0.42					43.36	40.36	
09321+10	0.39	0.25L	0.33L	0.93	2.87	42.73	39.72	44.27
11013-22	0.80	0.25L	0.25L	2.60	7.35	42.19	39.64	43.04
11203-02	0.69	0.25L	0.35L	1.92	4.07	44.24	41.48	45.01
11203-43	0.36	0.36L	0.25L	0.53	2.08	43.28	40.48	43.76
11206-43	0.46	0.28L	0.25L	1.05	2.49	43.27	40.79	43.94
13071-23	0.20	0.25L	0.25L	0.71	1.49	43.06	40.45	43.35
13220+06	0.46	0.25L	0.29L	0.67	1.99	43.58	40.38	44.00
13228-24	0.36	0.25L	0.31L	0.48	1.80	43.93	40.56	44.12
13301-24	0.80	0.28L	0.48L	0.82	1.96L	43.73	40.68	44.19
14255+01	0.61	0.30L	0.44L	0.75	1.25:	43.57	41.32	44.06
16065-28A	0.13	0.25L	1.12L	1.33	3.47	43.12	40.20	43.89L
16065-28B	0.09	0.25L	1.12L	1.33	3.47	43.11	39.94	43.88L
20459-22	0.45	0.26L	0.33L	0.95	1.33	43.77	40.76	44.14

TABLE III(a). H II region-like galaxies.

IRAS galaxy	z	FWHM [OIII]	FWHM H_α	[NII]/H_α	H_α/H_β	[OIII]/H_β	[SII]/H_α
01333-3452	.0225(6)		<89	0.47			
02566+0556	.0277(1)		92	0.48	6.9		0.3
03504-4440	.0054(1)	89	<91	0.11	3.5	3.1	0.3
04235-0840A	.103 (1)		630[a]				
04375-0900	.0165(8)		107				
04492-0618	.0149(2)	<124	99	0.36	3.8	0.6	0.2
04558-0952	.0136(2)		165	0.29			0.3
05123+0612	.0298(5)		<102	0.36			
05125+0612	.0148(3)		81	0.41	6.2		0.4
05409-2032	.0100(1)	113	95	0.22	5.2	2.0	0.4
05464-8208	.0189(8)		<110				
07224-7517	.0144(5)						
07427-5638	.0094(2)		187	0.38			0.4:
08538+1113A	.0297(8)		<86				
08538+1113B	.0293(8)		112				
09222-6327	.0106(1)	136	114		8.0	1.9	
09313+1113	.0085(1)	189	158	0.26	6.4	1.9	0.3
10240+0407	.0069(4)	<136	142	0.19			0.2[b]
11009-2248	.0036(3)		135	0.32	12.3		
11286+0455	.0332(1)	120	191	0.46	6.1	0.6	0.5
11508-1259	.0126(2)	150	182	0.27	6.4	0.8	
12190-3929	.0070(1)	178	<110	0.30	5.2	0.8	0.3
12252-2949	.0200(2)		183	0.44	11.2		0.3[b]
12336+1935N[c]	.0048(1)	158	129	0.18	5.4	2.5	0.4
12336+1935H[d]	.0046(2)	199	65		4.8	2.8	
12593-4913[e]	.0060(5)		<104	0.29			0.5[b]:
12594-4912[e]	.0060(5)						
13030-5002	.0117(8)		135	0.45			
13209+0639B	.0390(6)	<132	128		8.9	1.7	
13559+1442	.0127(1)	113	128	0.39	9.4	0.6	0.2[b]
14043-4809	.0100(2)	<110	<110	0.32	8.0	0.8	0.3
14069-2659B	.0201(3)	133	155	0.32	8.7	0.7	
14082-2647	.0232(3)		123	0.41	8.2		0.4
14546-8235	.0083(3)	<182	<108		4.4	2.2	
15421-7531	.0097(7)		113	0.50			
17353+1733	.0135(5)		136	0.34	6.3		0.4:
18159+1804	.0269(8)		<110	0.21	12.2		0.3[b]
19433-4028	.0191(5)		152	0.33			
19514-5507	.019 ?		<395				
20345-3539	.0195(1)	<129	<99	0.11	3.9	1.1	0.3
20562-5545	.0068(5)	95	91	0.16	5.3	0.5	0.4[b]
21140-3411	.0410(4)		<88				
21244-0945	.0229(5)		143	0.39			
21255-5259	.0029(3)	131	123	0.07:	4.2	2.4	
22028+0456	.0276(5)		94	0.48			
23328-1658	.0059(1)	155	123	0.19	5.1	2.7	0.4

Notes:
a) = Hα + [NII], spectrum obtained at the CTIO 1.5m telescope by M. Strauss
b) only [SII] λ6717Å measured
c) nucleus
d) bright HII region
e) two IRAS sources in the same galaxy.

TABLE III(b). H II region-like galaxies.

IRAS galaxy	b/a	Flux Densities (Janskys) 12μm	25μm	60μm	100μm	Log $L_{H\alpha}$	Log L_{IR}
01333-34	0.18	0.42L	0.35L	1.56	1.85:	40.23	44.20
02566+05	0.95	0.40L	0.26L	0.61	1.65L	41.15	44.13
03504-44	0.24	0.25L	0.25L	0.58	1.22	39.17	42.64
04235-08A	0.50						
04375-09	0.73	0.45L	0.25L	0.70	1.48	39.65	43.66
04492-06	0.18	0.25L	0.29:	2.43	5.27	40.38	44.15
04558-09	0.19	0.25L	0.25L	1.03	2.87	40.12	43.75
05123+06	0.38	0.56	0.25L	0.56:	1.21:	40.37	44.11
05125+06	0.74	0.25L	0.25L	1.41	2.34	40.65	43.86
05409-20	0.33	0.25L	0.25L	1.15	1.99	40.41	43.44
05464-82	0.83	0.32L	0.25:	1.04	3.66	40.38	44.05
07224-75	0.71:	0.25L	0.25L	0.69	2.39		43.68
07427-56	0.26	0.53L	0.27:	1.55	6.02	39.91	43.69
08538+11A	0.20	0.25L	0.34L	0.59	1.29:	40.33	44.13:
08538+11B	0.19	0.25L	0.34L	0.59	1.29:	40.68	44.11
09222-63	0.10	0.25L	0.25L	0.78	1.90	39.94	43.38
09313+11	0.98	0.26L	0.34L	0.69	1.25:	40.61	43.08
10240+04	0.45	0.25L	0.37L	0.69:	1.50	39.73	42.93
11009-22	0.31	0.42L	0.49	6.09	20.49	39.45	43.41
11286+04	0.96	0.54L	0.61L	0.41L	1.24	41.22	44.15
11508-12	0.23	0.25L	0.39L	0.50:	1.75	40.35	43.42
12190-39	0.47	0.25L	0.69L	2.59	5.63	39.52	42.51
12252-29	0.41	0.38L	0.40L	1.70	3.61	41.01	44.25
12336+19N[b]	0.87	0.25L	0.37L	1.20	2.56	39.67	42.85
12336+19H[c]	0.87					39.44	
12593-49[a]	0.20	1.44	0.62	0.40L	2.15	39.05	42.80
12594-49[a]	0.20	0.25L	0.25L	1.14	2.58:		43.04
13030-50	0.15	0.25L	0.25L	0.55	8.76:	39.75	43.88
13209+06B	0.82					40.85	
13559+14	0.36	0.25L	0.26L	0.95	2.22	40.45	43.45
14043-48	0.42	0.33L	0.25L	0.69	6.65L	40.05	43.04
14069-26B	0.67					40.90	
14082-26	0.33	0.25L	0.26L	1.16	1.93:	41.00	44.00
14546-82	0.69	0.25L	0.25L	0.44	1.73	39.32	42.32
15421-75	0.63	0.35:	0.40	2.98	8.85	39.81	43.92
17353+17	0.61	0.28L	0.25L	0.48L	1.01	40.00	43.36
18159+18	0.84	0.25L	0.26L	0.98	3.03	40.79	44.34
19433-40	0.63	0.25L	0.25L	1.04	2.31	40.55	43.99
19514-55	0.13	0.35L	0.25L	1.00	2.95	39.24	44.04
20345-35	0.87	0.25L	0.30L	1.61	1.51	42.01	44.07
20562-55	0.40	0.51L	0.61L	0.50:	1.48	39.51	42.83
21140-34	0.28	0.25L	0.32L	0.90	1.60:	40.55	44.56
21244-09	0.45	0.26L	0.25L	0.57	1.43	40.59	43.92
21255-52	0.12	0.25L	0.25L	0.93	1.44	39.37	42.22
22028+04	0.20	0.42L	0.25L	0.51	1.53	40.77	44.08
23328-16	0.22	0.25L	0.25L	0.96	1.56	40.07	42.87

Notes:
a) two IRAS sources in the same galaxy
b) nucleus
c) bright HII region.

TABLE IV. Galaxies with no detected emission lines.

IRAS galaxy	z_{abs}	Flux Densities (Janskys) 12μm	25μm	60μm	100μm	b/a	Log L_{IR}
01030-4636	.030 (4)	0.25L	0.66L	0.52:	1.03:	0.33	44.07
01049+0154		0.25L	0.78L	0.82	1.90	0.43	
01059-4621		0.25L	0.25L	0.43L	1.39	0.08	
03009-4826		0.84L	0.59L	0.45	0.85L	inter	
04088-5614	.003 (2)	0.74L	0.62L	0.41L	1.33	0.85	42.08
04362-2045	.031 (2)	0.44L	0.25L	0.40L	1.34	0.50	44.10
04400-2031	.005 (3)	0.25L	0.25L	1.06	3.48	0.88	42.93
06236-5622		0.25L	0.25L	0.64	0.40	0.33	
06494+1518A	.014 (3)	0.25L	0.25L	0.56	1.73	0.33	43.34
06494+1518B		0.25L	0.25L	0.56	1.73	0.63	
07351-6614[a]		0.31L	0.25L	0.44	1.26	0.80	
08190+0440		0.52	0.28L	0.40L	1.17L	0.71	
09263-3554A	.0154(7)	0.45L	0.49L	1.44	2.58	0.92	43.90
10165-0059		0.25L	0.27L	0.56	1.50	0.85	
11175-0246		0.25L	0.30L	0.59	1.60	0.80	
11272+0445		0.29L	0.45L	0.72:	1.90	0.44	
11468-5009		0.43L	0.25L	0.65	1.76	0.09	
12193-3942		0.53L	0.25L	0.89:	1.31:	0.77	
12547-4928		0.25L	0.25L	0.91	3.66	0.41	
13209+0639A		0.25L	0.25L	0.62	1.83	0.82	
13254-2422		0.25L	0.27L	0.61	1.86	0.37	
14069-2659A		0.25L	0.33L	0.49L	1.44	0.15	
14095-2710		0.25L	0.50L	0.48:	1.13	0.50	
14125-4724	.016 (3)	0.25L	0.25L	0.65	2.21	0.50:	43.74
15115-4009B	.0254(8)	1.05	0.43:	0.40L	1.99L	0.32	44.03
15159-3951		0.25L	0.39L	0.40L	1.89	0.15	
15347-4413		0.75	0.40:	0.67L	2.62L	0.95	
19244-5852		0.25L	0.25L	0.64	2.42	0.91	
20411-0324	.014 (3)	0.47	0.31L	0.40L	1.00L	0.48	
21138-0102		0.25L	0.30L	0.56	1.65	0.47	
22327-3737		0.26L	0.25L	0.47L	1.30	0.86	
23059+0423		0.25L	0.27L	0.65	1.41	0.74	
23168+1844		0.44L	0.25L	0.47	1.21	0.40	
23211+1917		0.25L	0.25L	0.97	1.72	0.76	
23220+0820		0.25L	0.26L	0.76	1.57L	0.21	

Notes:
a) spectra taken do not cover H_α region.

instrumental profile. To estimate the instrumental linewidth, comparison lamp (He–Ar) spectra were used; we measured the FWHM of a number of lines in the Hβ and Hα regions of these arc spectra and obtained a mean value of FWHM $= 5.0 \pm 0.5$ Å for the instrumental profile. Uncertainty in the redshift and FWHM is 30 km s^{-1} for spectra with high signal-to-noise ratio, becoming bigger for worse quality spectra. The accuracy of the redshift and FWHM is indicated in parentheses in column 3 of Tables I(a), II(a), and III(a). The line fluxes were not corrected for galactic extinction. The main source of uncertainty, especially in the case of weak lines, is the subjective choice of the local continuum for each line. Results of the line measurements are given in Tables I(a), II(a), and III(a).

b) Classification Criteria

Hα in emission is seen in 76% of the observed galaxies. To distinguish various activity levels of the objects on the basis of their optical spectra, two basic parameters are generally used, namely the width and relative intensity of the emission lines (see Veilleux and Osterbrock 1987 and references therein). As Sy 1 are characterized by the broad permitted lines, they are easy to identify. However, it is not always straightforward to classify objects with narrow emission lines. If it is a typical Seyfert 2, Liner, or H II-type nucleus, its characterization is quite simple. However, a large fraction of the observed galaxies have mixed properties. There are certainly situations where in an edge-on galaxy the nucleus is

highly obscured but a foreground H II region is not. In these cases the galaxies are possible to classify only with much better signal-to-noise ratio than obtained in our spectra.

For the distinction between Seyfert and starburst galaxies, e.g, Baldwin *et al.* (1981) adopted line ratios of [O III] λ 5007/H$\beta > 6$ and [N II] λ 6584/H$\alpha > 0.4$, for Seyferts, while Shuder and Osterbrock (1981) used [O III] λ 5007/H$\beta \geqslant 3$ and FWHM [O III] $\geqslant 300$ km s^{-1} as a qualifying criterion. On the other hand, Feldman *et al.* (1982) suggested that FWHM [O III] > 250 km s^{-1} is a good discriminator for AGN.

Veilleux and Osterbrock (1987) proposed that diagrams involving line ratios [O III]/Hβ, [N II]/Hα, [S II]/Hα, and [O I]/Hα are very useful in discriminating narrow line active galaxies from starburst ones. The Hβ emission line is almost always weak or absent in the observed spectra precluding the use of [O III]/Hβ as a discriminator. Another potentially useful line ratio is [S II]/Hα. However, the edges of our spectra are very noisy and the [S II] $\lambda\lambda$ 6717, 6731 lines are in general weak and difficult to measure.

To classify the objects we considered the line intensity ratio [N II] λ 6584/Hα and the widths of Hα and [O III], since they are the strongest lines observed in the spectra. The galaxies of the observed sample were then classified in three classes of nuclear activity level according to the following empirical criterion:

active galactic nuclei (AGN):

[N II] λ 6584/H$\alpha \geqslant 1.0$ and/or

FWHM ([O III] λ 5007, Hα) $\geqslant 300$ km s^{-1}

transition objects (Trans):

$0.6 \leqslant$ [N II] λ 6584/H$\alpha < 1.0$ and/or

$200 \leqslant$ FWHM ([O III], Hα) < 300 km s^{-1}

nuclear H II regions (H II):

[N II] λ 6584/H$\alpha < 0.6$ and

FWHM ([O III], Hα) < 200 km s^{-1}.

According to this classification scheme there are 28 AGNs, 39 transition objects, and 44 H II region-like galaxies. Properties of the three classes of galaxies (AGN, Trans, and H II) are listed in Tables I, II, and III, respectively. In Tables I(a) and II(a) we list the results of spectroscopic measurements as follows: Column 1: *IRAS* galaxy coordinates (1950); column 2: associated HEAO-1 source; column 3: redshift, uncertainties are quoted in parentheses; column 4: FWHM of [O III] λ 5007 in km s^{-1}; column 5: FWHM of Hα in km s^{-1}; columns 6, 7, 8, and 9: line intensity ratio of [N II] λ 6583/Hα, Hα/Hβ, [O III] λ 5007/Hβ, and ([S II] λ 6717 + 6731)/Hα, respectively. Table III(a) contains: column 1: *IRAS* galaxy coordinates (1950); column 2: redshift, uncertainties are quoted in parentheses; column 3: FWHM of [O III] λ 5007 in km s^{-1}; column 4: FWHM of Hα in km s^{-1}; columns 5, 6, 7, and 8: line intensity ratio of [N II] λ 6583/Hα, Hα/Hβ, [O III] λ 5007/Hβ, and ([S II] λ 6717 + 6731)/Hα, respectively.

Tables I(b), II(b), and III(b) include the following information: column 1: *IRAS* galaxy coordinate (1950); column 2: axial ratio measured from ESO Quick Blue films and photographic plates of POSS (Palomar Observatory Sky Survey); columns 3, 4, 5, and 6: flux densities (Janskys) at 12, 25, 60, and 100 μm, respectively, as given in Lonsdale *et al.* (1985); column 7: hard x-ray luminosity (2–10 keV) in erg s^{-1}, calculated using F_{Hx} from Wood *et al.* (1984); column 8: luminosity of Hα in erg s^{-1}; column 9: far-infrared luminosity (42.5 μ–122.5 μm in erg s^{-1}. F_{IR} taken from Lonsdale *et al.* (1985). We adopted the value $H_0 = 50$ km s^{-1} Mpc^{-1} and $q_0 = 0$.

Table IV contains information about the target galaxies with no detected emission lines. Column 1: *IRAS* galaxy coordinates (1950); column 2: redshift measured from absorption lines (Ca II, CH, Mg I, Na I); columns 3, 4, 5, and 6: flux densities (Janskys) at 12, 25, 60, and 100 μm, respectively; column 7: axial ratio, column 8: far-infrared luminosity. In Table V are the galaxies not observed: column 1: *IRAS* galaxy coordinates (1950); column 2: HEAO-1 source; columns 3, 4, 5, and 6: flux densities (Janskys) at 12, 25, 60, and 100 μm, respectively; column 7: axial ratio.

Figure 1 plots the spectra of all objects we classified as AGN and examples of spectra of the transition type and H II-region-like galaxies are in Fig. 2.

TABLE V. Galaxies not observed.

IRAS galaxy	HEAO-1 source	Flux Densities (Janskys) 12μm	25μm	60μm	100μm	b/a
01025+0153[a]	1H0102+017	1.56L	0.29L	1.01	2.64	?
05135+0603	1H0516+063	0.25L	0.25L	0.78	2.00	0.20
05137+0625	1H0516+063	0.42L	0.25L	0.57	1.91L	0.46
09079-3256	1H0908-326	0.25L	0.25L	0.74	2.03	0.79
12313-5922	1H1238-599	1.15	0.90	2.00:	7.21:	?
13036-4924	1H1304-497	0.60L	0.26L	0.55	1.67L	0.22
13212-2423	1H1325-246	0.55	0.27L	0.40L	1.03L	pec
15360-4423	1H1535-445	0.76	0.37	0.43L	3.70L	0.14
15405-6608	1H1532-662	0.45L	0.25L	0.54	1.96L	?

Note:
a) Dwarf galaxy (UGC 00668)

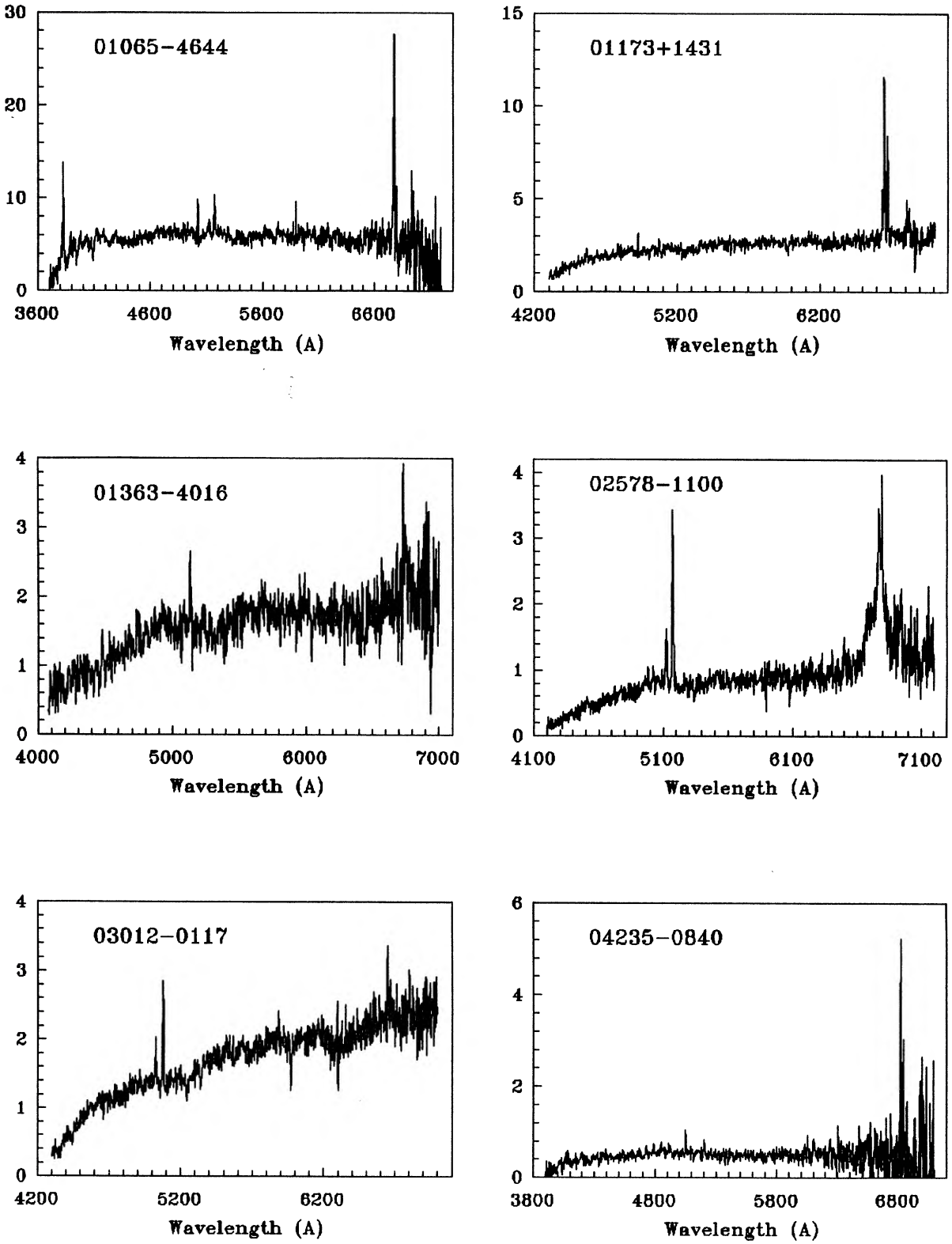

FIG. 1. Spectra of the 28 objects classified as AGN. Flux is in the y axis in units of 10^{-15} erg cm^{-2} s^{-1}.

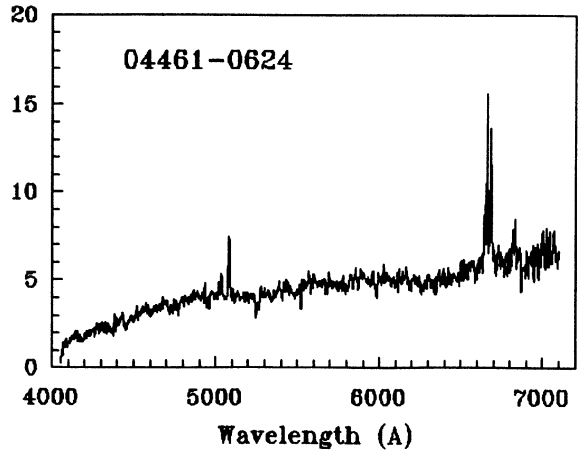

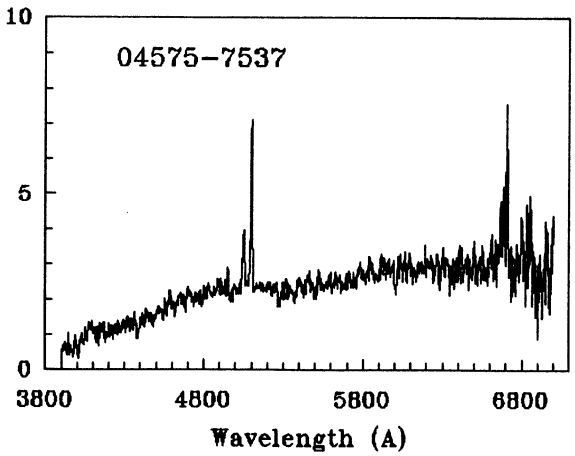

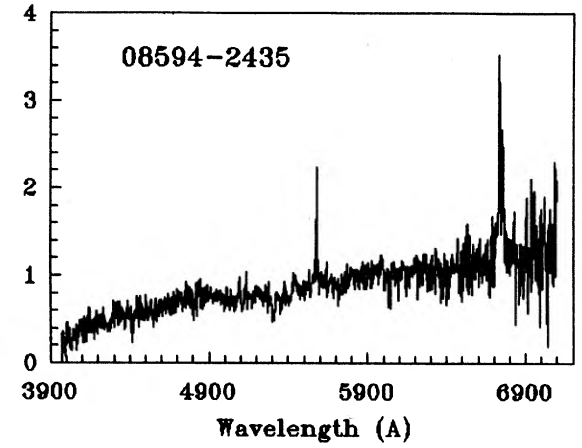

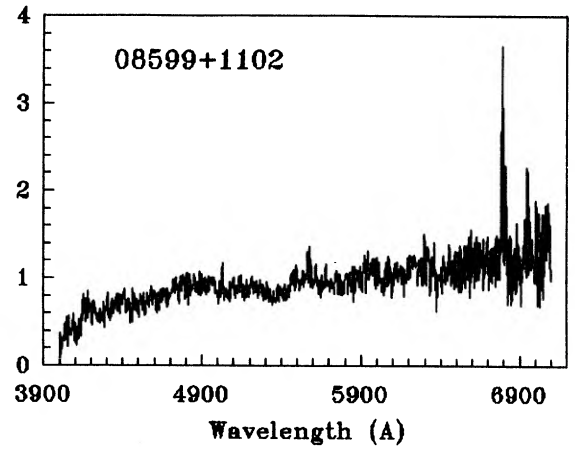

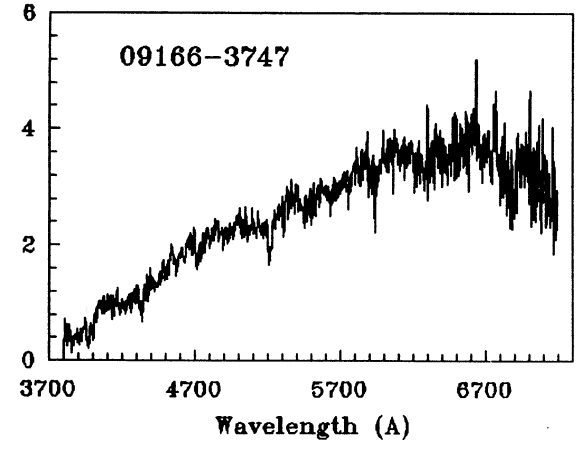

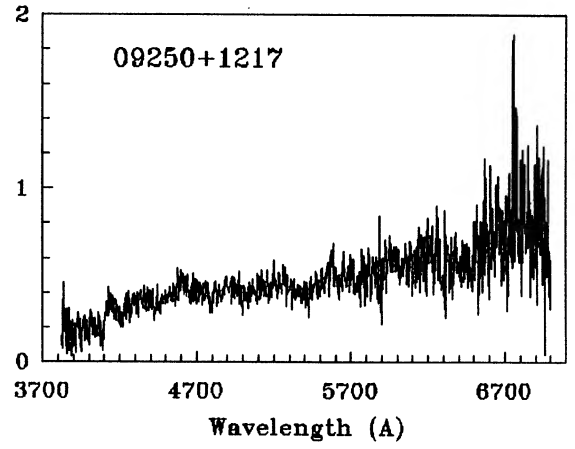

FIG. 1. (continued)

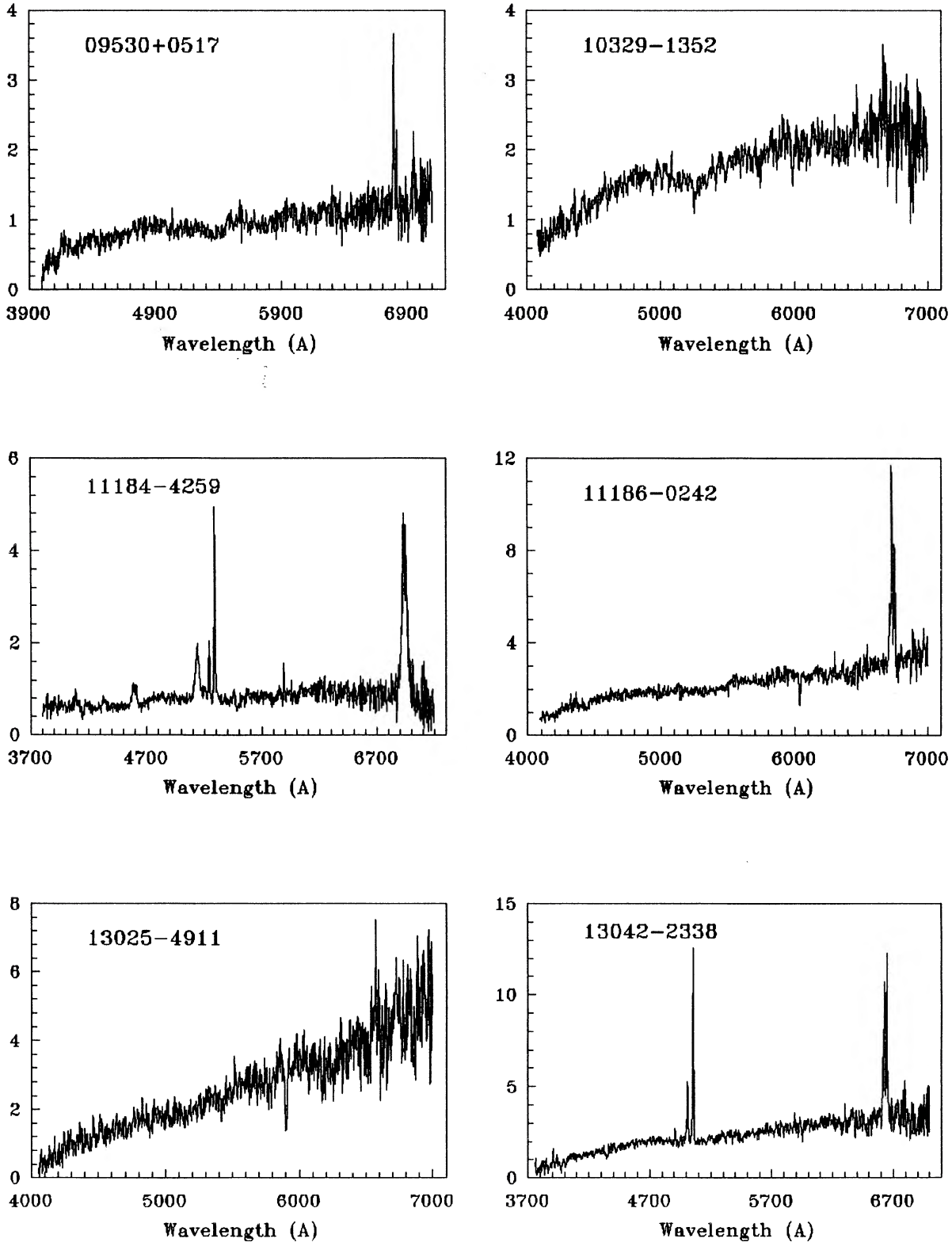

FIG. 1 (continued)

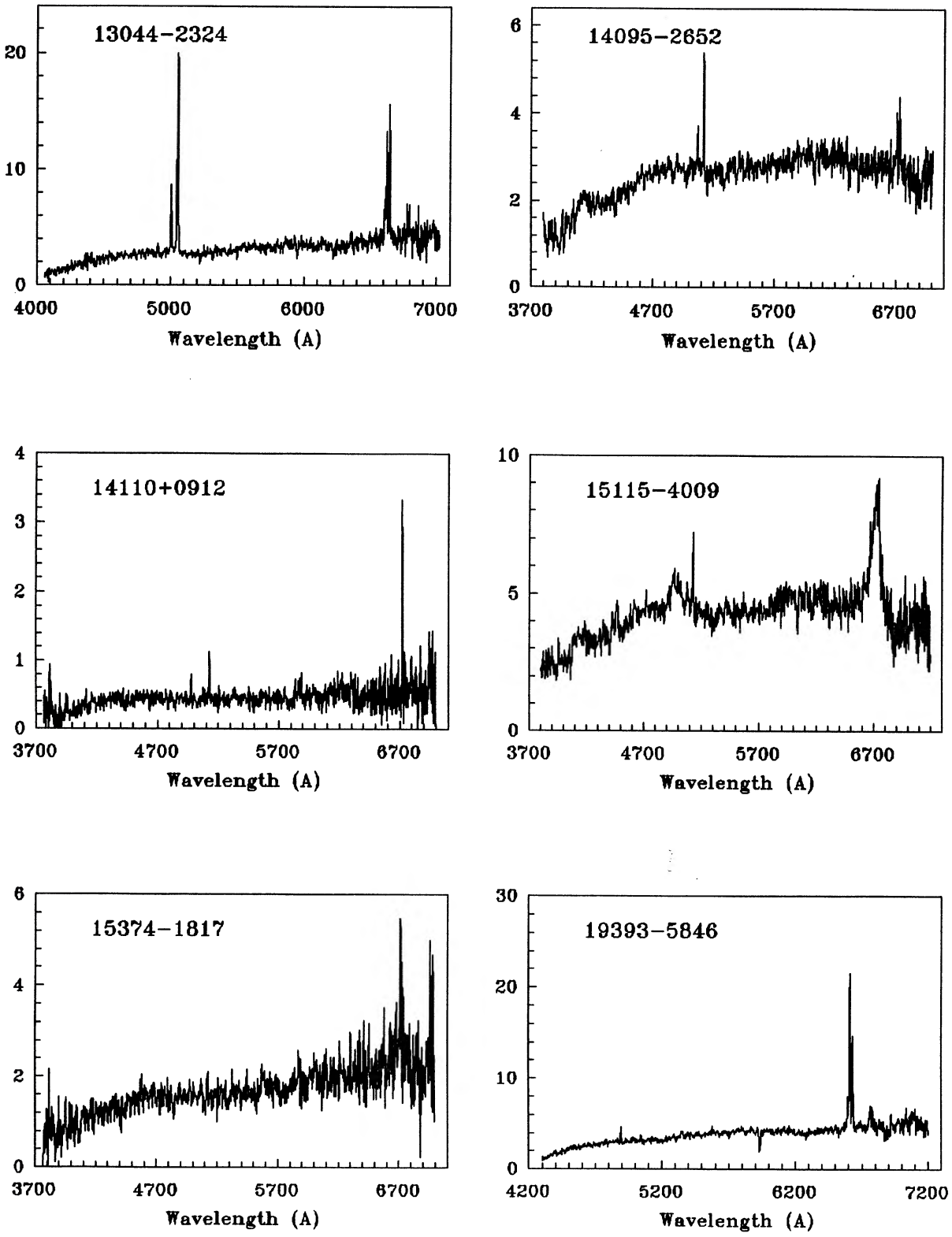

FIG. 1 (continued)

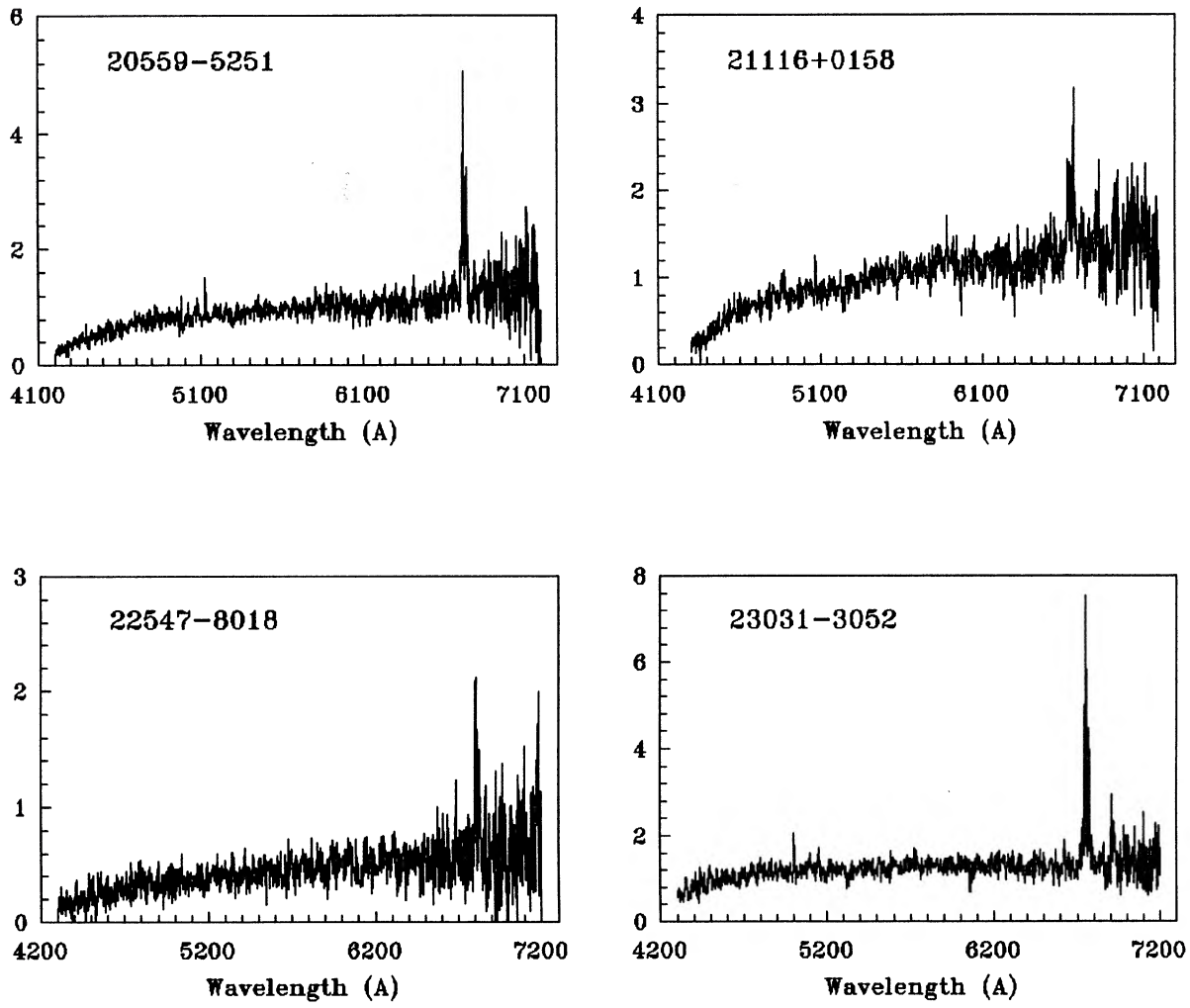

FIG. 1 (continued)

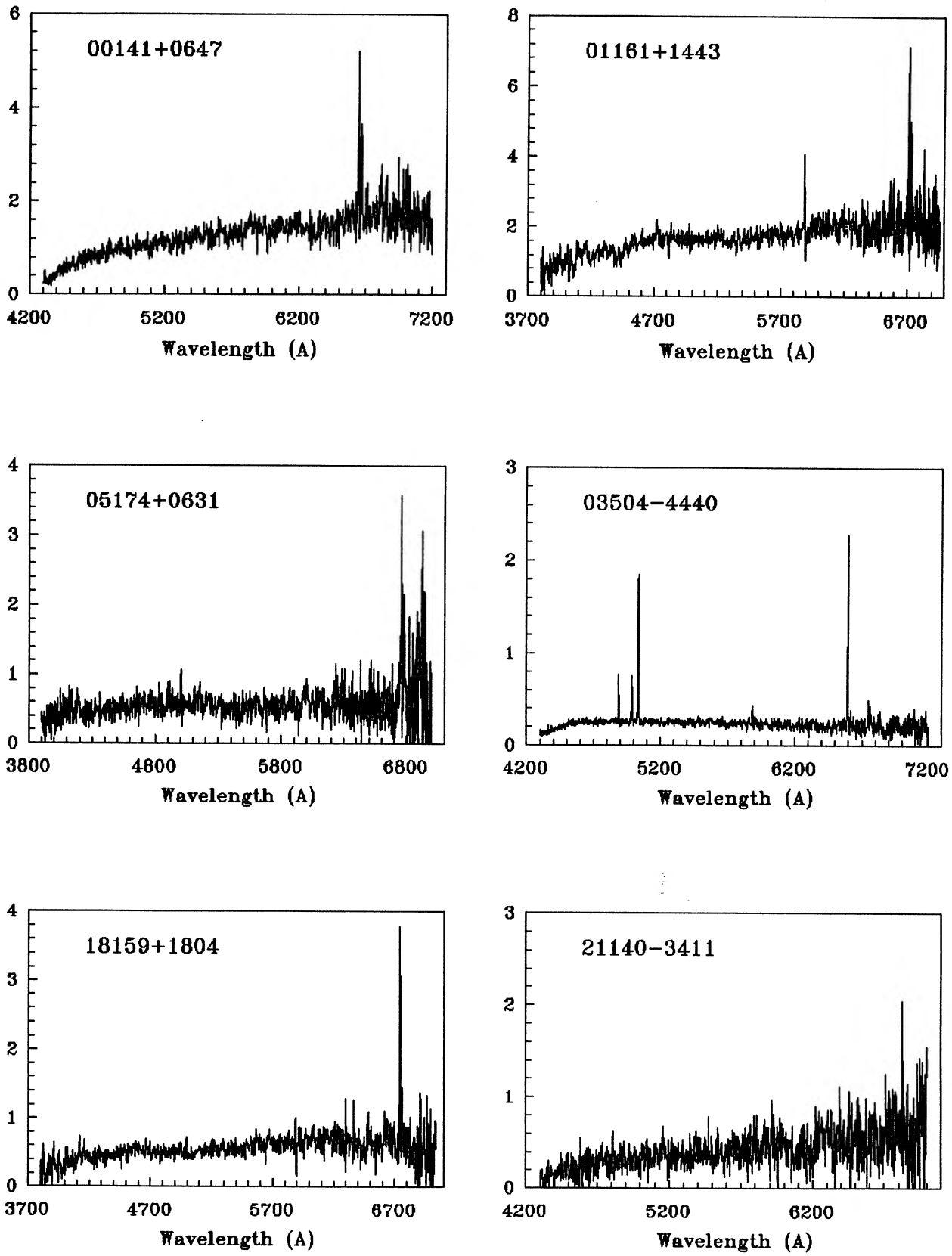

FIG. 2. Examples of the spectra of 3 transition type objects and 3 H II region-like galaxies. Flux is in the y axis in units of 10^{-15} erg cm^{-2} s^{-1}.

The FWHM of [O III] and Hα lines against [N II]/Hα is plotted in Fig. 3. This diagram is also representative of the distribution of the level of nuclear activity among the selected target galaxies. There are many galaxies for which the only emission line seen is Hα and they are not included in the figure.

Many galaxies in our sample are seen as edge-on and one could argue that a selection effect due to nuclear gas motions in the line of sight of the inclined galaxies accounts for the large number of broad emission-line galaxies seen in Fig. 3. This does not seem to be the case, since we do not find a correlation between FWHM and inclination of the galaxies.

The line intensity ratio [N II]/Hα and the FWHM are correlated with the infrared luminosity L_{IR} (total luminosity between 42.5 and 122.5 μm) as can be seen in Figs. 4 and 5. High infrared luminosity galaxies tend to have broader [O III] and Hα lines and higher [N II]/Hα ratio. The same mechanism that produces the nuclear radiation ionizes the gas, seems also to emit at least part of the far-infrared flux detected by *IRAS*. In Figs. 4 and 5 the nuclear H II-like galaxies occupy a region with low IR luminosity, very low [N II]/Hα ratio and narrow linewidths. It is interesting to see in Fig. 4 that the H II region-like galaxies form a sequence where higher infrared luminosity objects have higher excitation line ratio.

Evidence that the observed nuclei are heavily obscured is given by the steep Balmer decrements measured, which are much higher than the value predicted by the case B recombination theory.

c) Remarks on Specific Objects

In this section we will make some comments about some galaxies.

03018−5041. Edge-on spiral (ESO 199 − IG12) in interaction with a satellite galaxy.

04235−0840. Galaxy A is ~1.2 arcmin NE of a galaxy with extended halo, called galaxy B.

06494+1518. Two galaxies are close to this *IRAS* source coordinates: UGC 3578, called component B, and about ~2 arcmin SW of it, is Z0649.4 + 1518, denominated galaxy A.

07395−6755. Interacting system; component A is the one NW.

09250+1230. A double system in close interaction (Arp 237). Two nuclei are visible both with emission lines. The one to the NE is a AGN and the other is a transition-type object.

09263−3554 B. Interacting system at ~2.4 arcmin NE of

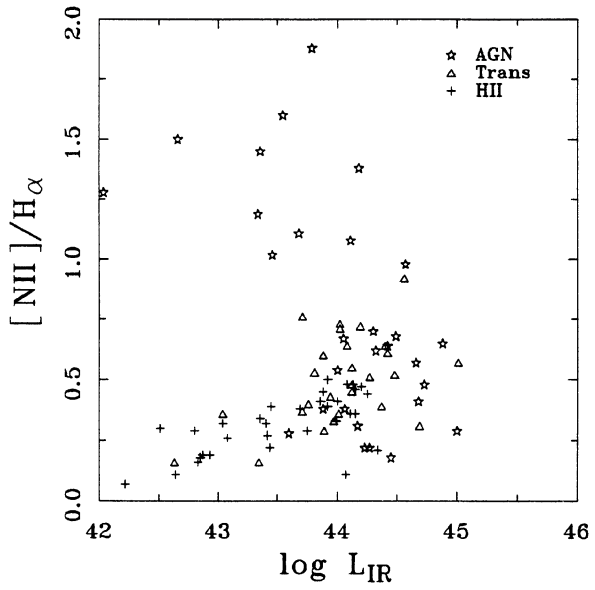

FIG. 4. [N II] λ 6584/Hα as function of the far-infrared luminosity for the three groups of line-emitting galaxies: Active galactic nuclei (AGN), transition objects (Trans), and H II-like galactic nuclei [H II].

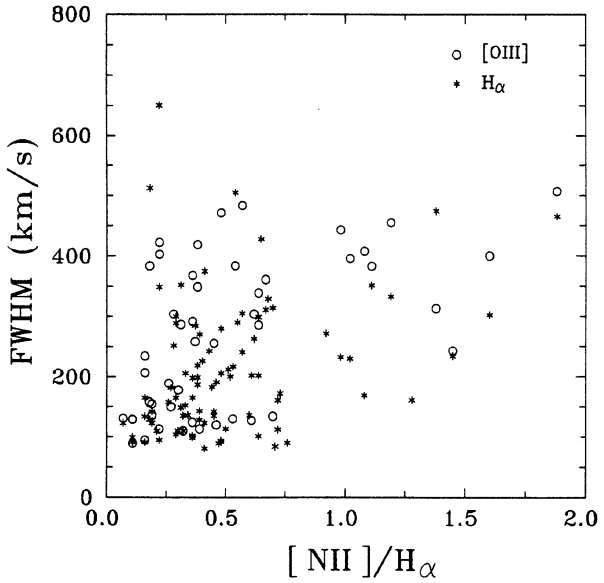

FIG. 3. FWHM of [O III] λ 5007 and Hα as function of [N II] λ 6584/Hα.

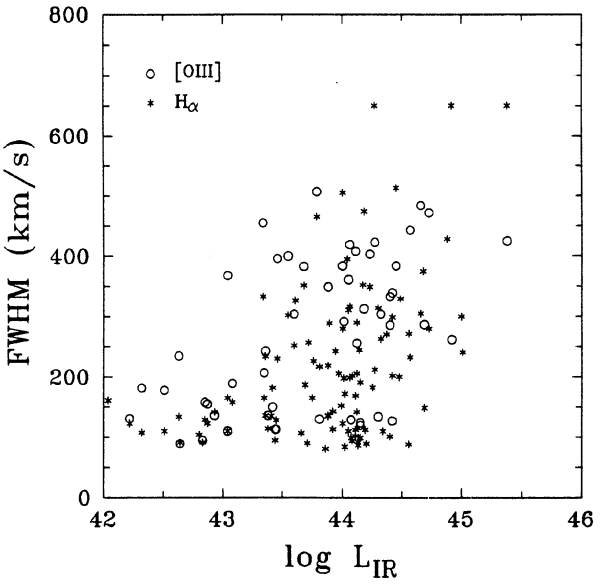

FIG. 5. FWHM of [O III] λ 5007 and Hα as function of the far-infrared luminosity.

the *IRAS* source 09263 − 3554. This later is an Sa galaxy with no detected emission lines.

11013−2258. Associated to NGC 3513, which is a transition-type galaxy ~74 kpc (~10.6 arcmin NW) away from NGC 3511 (*IRAS* source 11009 − 2248).

11184−4259 (ESO 265 − G23). This Seyfert 1 galaxy is a ringed spiral with a companion at about 126 kpc.

11203−0238. Compact galaxy in a cluster; there is a galaxy ~200 kpc away from it.

12336+1935. A peculiar galaxy with a bright H II region at the end of a kind of bar; the H II region is as bright as the nucleus and both have a very steep Balmer decrement.

13025−4911, 13028−4909. These two *IRAS* sources are in galaxy NGC 4945. This is a nearby edge-on galaxy with dust lane patches visible in the photographic plates; the nucleus was not seen at the 1 m telescope TV-guider camera. The spectrum obtained from its central region is underexposed. We verified later that NGC 4945 appears as a Seyfert galaxy in the catalog by Véron-Cetty and Véron (1989). The *IRAS* source associated with the active galactic nucleus is 13028 − 49, since its infrared colors are more typical of AGN than are the colors of the other source, 13025 − 49, which may be a giant H II region. The distance obtained for NGC 4945 is 7.2 Mpc; probably this is one of the nearest and least luminous AGN known.

13209+0639 B. NGC 5118 is associated to the *IRAS* source 13209 + 0639 and has no emission lines detected. The B component is at ~2.7 arcmin NE of NGC 5118 and has nuclear H II regions.

14069−2659 B. This galaxy is at ~1.3 arcmin SE of the *IRAS* source 14069 − 2659 which has no emission lines detected.

15115−4009. There are two galaxies at about the same redshift. The component A (ESO 328 − IG36), classified as a Seyfert 1 galaxy, has its major axis almost aligned to the N–S direction. The B component is ~4.2 kpc away (~1 arcmin NW) and its redshift was measured from absorption lines.

16065−2852. A group of three galaxies: component A has its major axis almost aligned with the E–W direction; galaxy B is ~84 kpc away and has its major axis almost aligned to the N–S direction.

IV. CONCLUSION

As a result of the present investigation we have obtained a sample of x-ray/infrared selected active galactic nuclei. Optical spectroscopy revealed that three of them are Seyfert 1 and 25 are narrow emission-line galaxies. It is quite surprising that the majority of the newly identified AGN are of type 2. We suggest three possible explanations:

(a) Previous surveys have recognized more Seyfert 1 than type 2 galaxies because their broad lines are easy to identify as is the strong ultraviolet excess.

(b) The more dust a galaxy contains, higher is the probability of obscuration. Therefore, the chance for them to appear as Sy 2 is also larger. At the same time, they will be strong infrared sources relative to optical and x-ray bands as compared to typical Sy 1 and will be easily detected by *IRAS*.

(c) On the average, Seyfert 1 are more luminous than are Seyfert 2. Many of the Sy 1 are at greater distances, appearing as stellar objects. In such cases they are not selected by our criteria because we only considered infrared sources identified as galaxies. We expect, for this reason, that within the flux limits we have taken, there remain various type 1 objects to be identified.

The narrow emission line AGN identified by us are similar to the x-ray-emitting Sy 2 first detected by Uhuru and Ariel V, although with lower fluxes. Examining the log N–log F_{Hx} distribution functions for SGs detected in the x-ray band (see Paper I) there is an obvious incompleteness of Sy 2 and objects seen edge-on as compared to Sy 1 and face-on. The inclusion of the newly identified AGN makes the sample of Sy 2 detected at the x-ray band fairly complete down to a limit of $\log F_{Hx} \sim -10.8$ (flux in ergs s^{-1}). Therefore, the x-ray luminosity function and space density of such objects can now be established. Luminosity function and statistical correlations involving the newly identified AGN will be presented in Paper III.

In Paper I we interpreted the excess of edge-on objects in the selected sample within the scenario of the obscuration hypothesis raised by Lawrence and Elvis (1982) (see also Mushotzky 1982). These authors also explained the existence of a class of narrowline x-ray emitting galaxies, with the same hypothesis. We interpret the present observations as an extrapolation of their conclusions to fainter limits.

Among other samples of x-ray selected AGN there are also signs of obscuration. Stocke *et al.* (1983) identified a group of x-ray AGN with narrow emission lines and very red colors, $B - V > +0.6$. However, Stephens (1989) and Kruper and Canizares (1989) claim that the majority of these objects are reddened due to the presence of a stellar component and not due to dust. In the Stocke *et al.* (1983), sample the reddish AGN have the lowest x-ray luminosities. There is also some evidence that low x-ray luminosity galaxies have large absorption columns (Lawrence and Elvis 1982; Mushotzky 1982).

Optical spectroscopy of 65 x-ray-selected AGN conducted by Stephens (1989) showed that x-ray selection may be an efficient way to find "narrow line Seyfert 1." It is worth pointing out that if the spectra obtained by Stephens were taken with lower signal-to-noise ratio, some of them would look like the AGN spectra obtained by us. All the AGN and transition objects we identified, except two (IRAS 13028 − 49 and IRAS 11013 − 22) have x-ray luminosities $L_{Hx} > 3 \times 10^{42}$ erg s^{-1}, in the range of the low-luminosity Sy 1 (Halpern and Oke 1987).

The main conclusion of this paper is that x-ray-emitting narrow line AGN are a common class of objects. We interpret these objects as being obscured Seyfert 1 as suggested by Mushotzky (1982), Lawrence and Elvis (1982), and Osterbrock (1984). As these authors have stressed and we emphasized in Paper I, the fact that they tend to the edge-on galaxies implies that the obscuring material is aligned with the disk of the galaxy.

We are grateful to the CTIO for hospitality and use of its facilities. The excellent assistance of the mountain crew was really appreciated. Many thanks to M. M. Phillips for helpful discussions and to S. R. Heathcote for assistance with the 2D-Frutti and data reduction. It is a pleasure to thank H. Andernach for helpful comments and suggestions. S. D. K. acknowledges a fellowship from CNPq (200552/87.2).

REFERENCES

Baldwin, J. A., Phillips, M. M., and Terlevich, R. (1981). Publ. Astron. Soc. Pac. **93**, 5.

Baldwin, J. A., and Stone, R. P. S. (1984). Mon. Not. Astron. Soc. **206**, 241.

Bradt, H. V., Burke, B. F., Canizares, C. R., Greenfield, P. E., Kelly, R. L., McClintock, J. E., and van Paradijs, J. (1978). Astrophys. J. **226**, L111.

Carter, D. (1984). Astr. Express **1**, 61.

de Grijp, M. H. K., Miley, G. K., and Lub, J. (1987). Astron. Astrophys. Suppl. **70**, 95.

de Grijp, M. H. K., Miley, G. K., Lub, and de Jong, T. (1985). Nature **314**, 240.

Elvis, M., Maccacaro, T., Wilson, A. S., Ward, M. J., Penston, M. V., Fosbury, R. A. E., and Perola, G. C. (1978). Mon. Not. R. Astron. Soc. **183**, 129.

Feldmann, F. R., Weedman, D. W., Balzano, V. A., and Ramsey, L. W. (1982). Astrophys. J. **256**, 427.

Halpern, J. P., and Oke, J. B. (1987). Astrophys. J. **312**, 91.

Kailey, W. F., and Lebofsky, M. J. (1988). Astrophys. J. **326**, 653.

Keel, W. C. (1980). Astron. J. **85**, 198.

Kirhakos, S. D. (1986). Masters Thesis, Universidade de São Paulo.

Kirhakos, S. D., Steiner, J. E. (1990a). Astron. J. (Paper I) (in press).

Kirhakos, S. D., and Steiner, J. E. (1990b). In preparation (Paper III).

Kruper, J. S., and Canizares, C. R. (1989). Astrophys. J. **343**, 66.

Lawrence, A., and Elvis, M. (1982). Astrophys. J. **256**, 410.

Lonsdale, C. J., Helou, G., Good, J. C., and Rice, W. (1985). *Cataloged Galaxies and Quasars Observed in the IRAS Survey* (Jet Propulsion Laboratory, Pasadena).

Low, F. J., Huchra, J., Kleinmann, S. G., and Cutri, R. M. (1988). Astrophys. J. Lett. **327**, L41.

Miley, G. K., Neugebauer, G., and Soifer, B. T. (1985). Astrophys. J. **293**, L11.

Nushotzky, R. F. (1982). Astrophys. J. **256**, 92.

Osterbrock, D. E. (1984). Q. J. R. Astron. Soc. **25**, 01.

Osterbrock, D. E., and de Robertis, M. M. (1985). Publ. Astron. Soc. Pac. **97**, 1129.

Schnopper, H. W., Delvaille, J. P., Epstein, A., Cash, W., Charles, P., Bowyer, S., Hjellming, R. M., Owen, F. N., and Cotton, W. D. (1978). Astrophys. J. **222**, L91.

Shuder, J. M. (1980). Astrophys. J. **240**, 32.

Shuder, J. M., and Osterbrock, D. E. (1981). Astrophys. J. **250**, 55.

Stephens, S. A. (1989). Astron. J. **97**, 10.

Stocke, J. T., Liebert, J., Gioia, I. M., Griffiths, R. E., Maccacaro, T., Danziger, I. J., Kunth, D., and Lub, J. (1983). Astrophys. J. **273**, 458.

Stone, R. P. S., and Baldwin, J. A. (1983). Mon. Not. R. Astron. Soc. **204**, 347.

Veilleux, S., and Osterbrock, D. E. (1987). Astrophys. J. Suppl. Ser. **63**, 295.

Véron, P., Lindblad, P. O., Zuiderwijk, E. J., Véron, M. P., and Adam, G. (1980). Astron. Astrophys. **87**, 245.

Véron-Cetty, M. P., and Véron, P. (1989). *A Catalogue of Quasars and Active Galactic Nuclei*, ESO Scientific Report No. 7 (4th edition).

Ward, M. J., Wilson, A. S., Penston, M. V., Elvis, M., Maccacaro, T., and Tritton, K. P. (1978). Astrophys. J. **223**, 788.

Wilson, A. S. (1979). Proc. R. Soc. London, A. **366**, 461.

Wood, K. S., Meekins, J. F., Yentis, D. J., Smathers, H. W., McNutt, D. P., Bleach, R. D., Byran, E. T., Chubb, T. A., Friedman, H., and Meidav, M. (1984). Astrophys. J. Suppl. Ser. **56**, 507.